Modulation of Pore Shape and Adsorption Selectivity by Ligand Functionalization in a Series of "rob"-like Flexible Metal-Organic Frameworks

Javier Cepeda,[a] Manuel Pérez-Mendoza,[b] Antonio J. Calahorro,[b] Nicola Casati,[c] José Manuel Seco,[a] Marta Aragones-Anglada,[d] Peyman Z. Moghadam,[d] David Fairen-Jimenez[d,*] and Antonio Rodríguez-Diéguez[b,*]

We report the synthesis of a new family of four new isoreticular metal-organic frameworks (MOFs) based on Cu-Cu paddle-wheel building units. The four MOFs contain 1D microchannels modulated by chemical functionalisation of the dicarboxylate ligand or the use of different bis-4,4'-pyridyl-like connectors behaving as ancillary linkers. A deep analysis of their CO_2, H_2 and CH_4 adsorption properties, combining both experimental and grand canonical Monte Carlo isotherms as well as in-situ synchrotron X-ray diffraction, shows variable adsorption behaviour towards the studied gases, with some materials acting as molecular sieves with virtually infinite selectivity.

Introduction

Metal-organic frameworks (MOFs) are one of the most exciting advances in recent porous materials science, showing tunable porosities and a wide range of properties for specific applications, including gas adsorption, separation and healthcare.[1] With more than 80,000 structures synthesised so far according to the Cambridge Crystallographic Database Centre,[2] MOFs possess a unique structural and topological diversity.[3] Indeed, they have broken all limits of specific accessible surface area, with BET areas reported up to 8,000 $m^2\ g^{-1}$, and as such have revolutionized the field of porous materials.[4] MOFs consist of self-assembled organic ligands and metal ions or clusters organized into secondary building units (SBUs). Given their modular structure, the porosity can be in principle modulated or functionalized just by slightly modifying the chemistry, shape and length of the ligands.[5] In this sense, SBUs based on Cu-Cu paddle-wheel cores found in the prototypical HKUST-1 MOF are widely known to build rigid and porous MOFs.[6] Also, some topologies allow the coordination of long ancillary linkers replacing solvent molecules at the axial positions in the pristine structure, which may serve as a valid strategy to give open architectures.[7]

The development of porous materials is many times linked to the storage and separation of small gas molecules such as H_2, CO_2 and CH_4.[8,1j] Of particular interest are adsorbents showing high affinity for CO_2 so they can be applied to carbon capture technologies[9] and purification of natural gas streams[10] as well as H_2 in syngas mixtures.[11] In terms of adsorption behaviour, most MOFs are characterized by their microporous crystalline nature, with uniform void networks that usually show Type I adsorption isotherms.[12] Interestingly, and in contrast with classical porous materials such as zeolites and activated carbons, MOFs have also shown other unusual shapes and steps in terms of adsorption isotherms, such as Types IV and VI.[3a,12] The occurrence of unusual shapes during the adsorption process has been considered key to designing appropriate adsorbents for gas separations. These uncommon adsorption processes have been observed not only when MOFs contain cavities with different sizes or preferred adsorption sites[13] but also when they consist of flexible backbones allowing gate opening,[14] breathing[15] or swing effect.[16]

We recently reported a $[Cu_2(COO)_4]$ paddle wheel-based MOF (**GR-MOF-1**, $\{[Cu_2(\mu_4\text{-glu})_2(\mu\text{-bpp})]\cdot 2H_2O\}_n$) (glu = glutarate, bpp = 1,3-bis(4-pyridyl)propane) showing Type IV CO_2 isotherms and a remarkable selectivity towards CO_2 versus CH_4.[17] Moreover, N_2 adsorption revealed a non-porous behaviour which, unlike commonly attributed causes (e.g. incomplete solvent removal, crystal collapse, or massive presence of impurities),[18] seems to origin at inherent surface

[a] *Departamento de Química Aplicada, Facultad de Química, Universidad del País Vasco/Euskal Herriko Unibertsitatea (UPV/EHU), 20018 San Sebastián, Spain.*
[b] *Departamento de Química Inorgánica, Universidad de Granada, 18071 Granada, Spain.*
[c] *Paul Scherrer Institute, 5232 Villigen, Switzerland.*
[d] *Adsorption & Advanced Materials Laboratory (AAML), Department of Chemical Engineering & Biotechnology, University of Cambridge, United Kingdom. *E-mail: df334@cam.ac.uk.*

† Electronic Supplementary Information (ESI) available: Synthesis, PXRD, TGA, FTIR, PL characterisation, details on molecular simulations. CCDC 1836112-1836115. See DOI: 10.1039/x0xx00000x

instability generated by structural defects. We attributed this behaviour to the flexibility provided by glu ligand and/or the existence of structural defects on the external surface. Taking the conformational freedom of the glu ligand as a reference, we hypothesised that introducing subtle modifications on it, e.g. including different functional groups, or combining it with other bis-4,4'-pyridyl-like ancillary linkers, could be a promising strategy to tune its behaviour in order to design analogous materials with enhanced selective gas adsorption capacities, but in contrast with the original **GR-MOF-1**, are able to adsorb CO_2 at lower pressures. Herein, we report the synthesis and adsorption properties of an isoreticular series of MOFs based on **GR-MOF-1,** obtained using three ancillary ligands with planar geometry (Scheme 1). Incorporation of these ligands resulted on four new MOFs, namely $\{[Cu_2(\mu_4\text{-glu})_2(\mu\text{-azpy})]\cdot 4H_2O\}_n$ (**GR-MOF-2**), $\{[Cu_2(\mu_4\text{-meglu})_2(\mu\text{-bpdb})]\cdot 5H_2O\}_n$ (**GR-MOF-3**), $\{[Cu_2(\mu_4\text{-dmglu})_2(\mu\text{-bpdb})]\cdot 4H_2O\}_n$ (**GR-MOF-4**), and $\{[Cu_2(\mu_4\text{-meglu})_2(\mu\text{-bpo})]\cdot 4H_2O\}_n$ (**GR-MOF-5**) (meglu = 2-methylglutarate, dmglu = 2,2'-dimethylglutarate, azpy = 4,4'-azopyridine, bpdb = 1,4-bis(4-pyridyl)-2,3-diaza-1,3-butadiene, bpo = 2,5-bis(4-pyridyl)-1,3,4-oxadiazole).

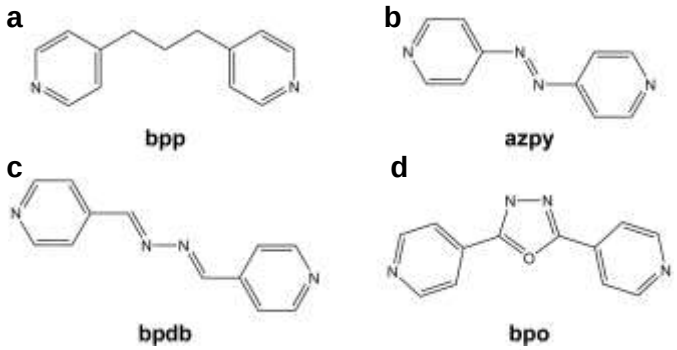

Scheme 1. Employed planar bis-4,4'-pyridyl-like ancillary linkers: **a)** bpp (used for **GR-MOF-1**), **b)** azpy (**GR-MOF-2**), **c)** bpdb (**GR-MOF-3** and **GR-MOF-4**), and **d)** bpo (**GR-MOF-5**).

Results and discussion

We obtained single crystals of the four MOFs by slow evaporation of water solutions containing equimolar amounts (0.25 mmol) of copper(II) sulphate, the corresponding dicarboxylic acid and the bis-4,4'-pyridyl-like linker (see section S3 in ESI). Their purity was confirmed by elemental analysis, thermogravimetry (TG/DTA), infrared (see ESI) and powder X-ray diffraction (PXRD), as described below.

Structural descriptions

All compounds crystallized in the *C*2/c space group and consist of 3D frameworks sustained by Cu-Cu paddle-wheel SBUs in such a way that they preserve the **rob** topology characteristic of **GR-MOF-1**. Within the centrosymmetric SBUs, four bridging carboxylate moieties bring two symmetry-related Cu1 atoms together imposing Cu···Cu distances of *ca.* 2.6 Å. The slightly distorted square-pyramidal NO_4 environments (S_{SPY} of *ca.* 0.55, see S4 section in ESI) formed around copper(II) atoms are completed by the nitrogen atoms belonging to the bis-4,4'-pyridyl-like linkers, which occupy the axial positions. Figure 1 represents the growth of the 3D network; Tables S2-5 show the coordination bond lengths of the reported **GR-MOFs**. The Cu-Cu paddle-wheel units are linked by means of the μ_4-dicarboxylic connectors, in such a way that each SBU joins four neighbouring ones, leading to 2D Cu-glu layers with distorted square grids that spread along the crystallographic *bc* plane. A remarkable feature of these layers is their corrugated shape, which modulates according to the geometry of the dicarboxylate ligand.

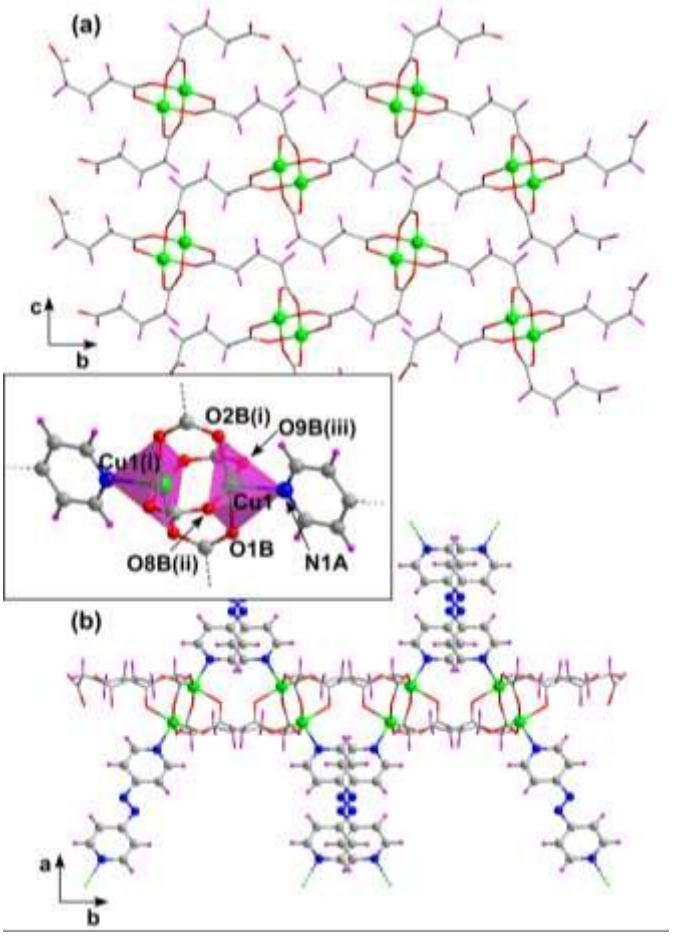

Fig. 1. a) View of the Cu-glut layer of **GR-MOF-2** showing the distorted square grid (azpy have been omitted for clarity). **b)** Disposition of azpy ligands arising from the Cu-glut layer. Inset: dimeric SBU with the general numbering scheme.

Looking at the structure of the four GR-MOFs, it is remarkable how the presence of methyl groups in the aliphatic chain of glu ligand force it to acquire a more folded conformation, which brings a lengthening in the distance among adjacent SBUs. In fact, the distance between centroids of SBUs are 7.78-7.84 (glu) < 8.09 (meglu) < 8.20 Å (dmglu). Hereafter, almost planar bis-4,4'-pyridyl-like linkers emerge from the corrugated layers and serve as pillars by bringing the layers together to build the 3D framework with ($4^8{\cdot}6^6{\cdot}8$) point symbol. It is worth noticing that, given the twisted orientation of the dimeric SBUs within the layer, the pillaring linkers do not arise parallel to the mean *bc* plane of the layer but they form an angle of 52.3-60.8°, taking into account the mean plane of the

azpy, *bpdb* and *bpo* ligands. As a result, all architectures show a corrugated arrangement along the [0 1 0] axis resembling an accordion, similar to that described for **GR-MOF-1**.[17] This geometry is particularly interesting since we hypothesise that it may, in principle, promote similar adsorption behaviour than that observed previously (Figure S7).

Structural geometry and adsorption performance

We first characterized the pore size distributions (PSD) of these four MOFs through a Monte Carlo procedure that explores the free volume with a probe of incremental size (Figure S13).[18] Figure 2 shows the microchannels with sections of 6.7 Å, 7.2, 7.0 and 6.8 Å respectively for **GR-MOF-2, -3**, **-4** and **-5** when the solvent molecules are removed (see also Figures S8–11). It is worth mentioning that, among the four studied MOFs, **GR-MOF-2** displays comparatively narrower and less cylindrical microchannels attributed to a more corrugated geometry of the *meglu* ligand. Taking into account these pore sizes, all MOFs should adsorb small gas molecules such as CO_2 and CH_4. Figure S1 shows the TG/DTA, which proves that the activation process did not affect the integrity of the MOFs; PXRD on the activated samples confirmed that the materials were able to retain their structural integrity (Figures S2-6). As detailed below, herein reported **GR-MOFs** exhibit similar adsorption performance compared to **GR-MOF-1**, giving non-porous behaviour against N_2 but excellent selectivity when exposed to CO_2. This kind of discrepancies have been observed before by different groups, including ourselves,[17,19,20] as in the work by Matzger et al. on the porous Zn-HKUST-1 MOF. In it, positron annihilation lifetime spectroscopy confirmed that the lack of gas uptake at 77 K in the material was caused by the inherent surface instability after solvent removal, which created a diffusion barrier that made the material non-permeable to guest molecules.[21]

Adsorption isotherms of N_2 at 77 K revealed non-porous materials in these conditions. In spite of that, we decided to measure the adsorption isotherms of CO_2 and CH_4 at 273 K and H_2 at 77 K and high pressure for all the MOFs reported here. Figure 3a shows the experimental isotherms for CO_2 in the four MOFs, Figure 3b shows the comparison of the experimental isotherms of CO_2, CH_4 and H_2 on **GR-MOF-2** and Figure S14 shows the CH_4 and H_2 adsorption isotherms for the remaining MOFs; Table 1 summarises the adsorption capacities, geometric surface area using molecular simulations and crystal density. Interestingly, the four MOFs show remarkably different adsorption behaviours. First, all the MOFs were able to adsorb CO_2, showing Type IV isotherms, where the first step is related to the microporosity and the adsorption after the plateau is related to CO_2 condensation, probably in the interstitial space between particles. At saturation levels (*ca.* 25 bar), the CO_2 capacity of **GR-MOFs** follows the trend **3** ≈ **2** < **5** < **4**, with uptakes of 9.02, 9.54, 13.64 and 15.29 wt.% (Table 1), or 4, 4, 6 and 8 molecules per unit cell, respectively. These storage capacities can be considered as moderately high, and comparable to those obtained for some reference MOFs such as MIL-96(Al) and MIL-102 (18.6 and 13.0 wt.%, respectively).[22] When studying other gases, **GR-MOF-2** shows no adsorption of CH_4 in the whole range of pressures and no adsorption of H_2 below 1 bar (Figure S15), followed by a step that plateaus at 0.14 wt.%, similar to the gate opening mechanism found in other MOFs (Fig. 3b).[23] **GR-MOF-3**, on the other hand, does adsorb CH_4 (0.94 wt.% capacity at 25 bar) but does not adsorb H_2, whereas **GR-MOF-4** does not adsorb any H_2 or CH_4 (Figure S14). Finally, **GR-MOF-5** adsorbs H_2 (0.53 wt.% at 25 bar) and CH_4 (1.20 wt.% at 25 bar).

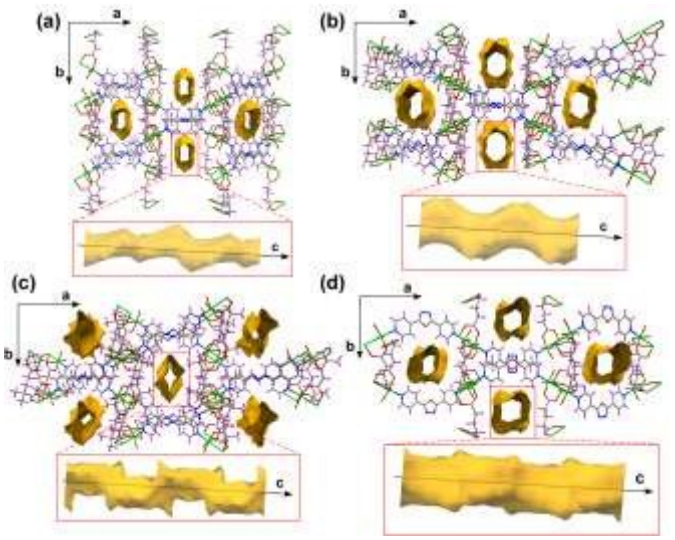

Fig 2. Crystal packings of the 3D frameworks of **a) GR-MOF-2, b) -3, c) -4** and **d) -5** showing the one-dimensional microchannels along the [0 0 1] direction (probe size = 3.65 Å).

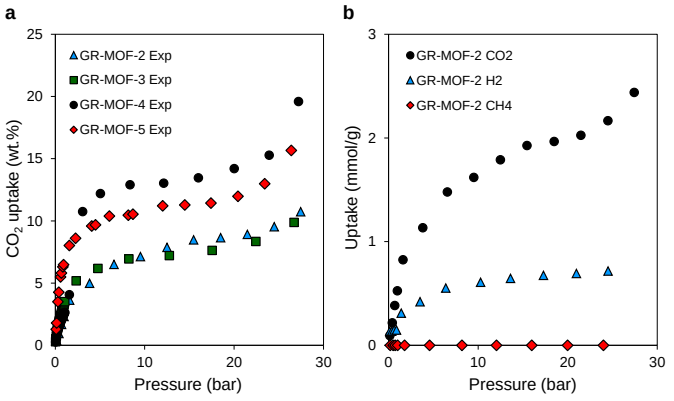

Fig. 3. a. Experimental CO_2 adsorption isotherms at 273 K on all the GR-MOFs. **b.** CO_2, H_2 and CH_4 adsorption isotherms for **GR-MOF-2**; CO2 and CH_4 are measured at 273 K and H_2 at 77 K.

Table 1. CO_2, CH_4 and H_2 adsorption capacity of GR-MOFs, geometric surface area (S_a) and crystal density (ρ_c).

	CO_2 wt.%	CH_4 wt.%	H_2 wt.%	S_a m^2/g	ρ_c g/cm^3
GR-MOF-2	9.54	0	0.14	740	1.39
GR-MOF-3	9.02	0.94	0	804	1.34
GR-MOF-4	15.29	0	0	845	1.28
GR-MOF-5	13.64	1.20	0.53	747	1.40

To understand the adsorption phenomena in these MOFs, we monitored the evolution of the unit cell parameters in situ using synchrotron radiation during the adsorption of CO_2 at 273 K and up to 50 bar – we focus here on a powder sample of **GR-MOF-2.** Figure S16 shows the variation of the unit cell parameters when increasing the adsorption pressure. Initially, the microchannels are slightly compressed at low pressures (from 0 to 5 bar) as inferred from the decrease of the *a* parameter and the moderate increase of *b* and *c* parameters. All in all, it brings a contraction of *ca.* 0.4% in the cell volume. Upon raising the pressure, the trend is inverted regarding the *a* parameter while the channels get filled with CO_2 molecules. The analysis of the PSD on the **GR-MOF-2** structures generated by changing the unit cell parameters confirms the reduced impact of these changes in the pore geometry, where the pore diameter did not change significantly (Figure S13).

Once the existence of significant flexibility upon adsorption has been discarded, the only alternative explanation for the gas adsorption selectivity observed here is the existence of defects in the external surface of the MOF, which prevents the adsorption of certain gases in the porosity – similar to the Zn-HKUST-1 case.[24] The reason why some gases can be adsorbed or not will be related in turn to their size, shape and interaction with the host material. At this point, we used grand canonical Monte Carlo (GCMC) simulations to predict the adsorption performance of these MOFs, in order to compare their adsorption isotherms on pristine, perfectly activated samples, to those obtained experimentally in real materials. It is worth reminding that in GCMC simulations, the insertion of molecules in the porosity does not take into account the pathway a molecule needs to follow to get adsorbed. In other words, the molecular simulation does not distinguish between open and closed porosity. Figure 4 shows the comparison of CO_2 experimental and GCMC simulated isotherms on **GR-MOF-2** – the simulated curve has been scaled down (ϕ=0.52) to match the plateau in the experimental curve. This scaling factor allows to include the existence of denser phases – present in experimental, real samples – on the molecular simulations. Figure S17 shows the simulated isotherms for CO_2, CH_4 and H_2 for the four MOFs, proving that the four MOFs are theoretically porous for the four structures. Figure S18 shows the comparison between experimental and simulated, scaled isotherms for CO_2 for the four MOFs. Interestingly, while the experimental isotherm shows an important hysteresis (shown for GR-MOF-2), probably due to the existence of kinetic effects in the adsorption and desorption equilibrium, the simulated isotherm goes between both experimental adsorption and desorption branches. It is important to highlight that GCMC simulations will not be able to distinguish between accessible and closed porosity or the existence of such kinetic effects.

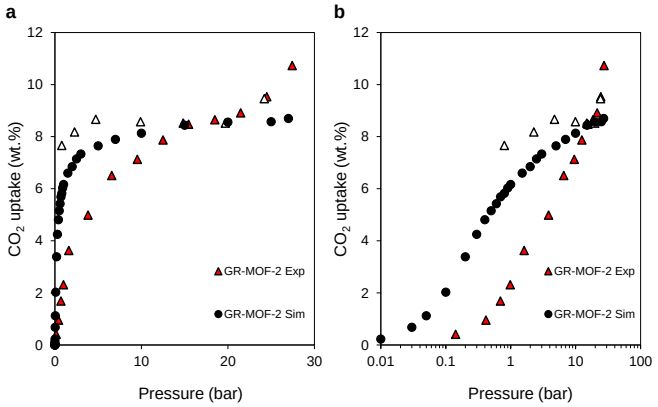

Fig. 4. Comparison of CO_2 adsorption isotherms at 273 K on GR-MOF-2: experimental adsorption, red triangles, and desorption, empty triangles, as well as simulated, black circles. **a.** linear and **b.** semi-logarithmic scale.

At this point, we took into account the observed changes during the in situ experiments on GR-MOF-2 by extending the simulations to four new structures based on the original one. The first two, GR-MOF-2-5bar and GR-MOF-2-10bar were obtained from the original **GR-MOF-2**, but changing the unit cell parameters according to the in situ studies measured at 5 and 25 bar, respectively, without further changes. We included two additional structures, GR-MOF-2-5bar-Opt and GR-MOF-2-25bar-Opt, where we relaxed the structures using a combination of a cascade of the steepest descent, adjusted basis set Newton–Raphson, and quasi-Newton methods – as implemented Forcite module of in Materials Studio. Figure 5 shows the comparison of the GCMC simulated CO_2 isotherms

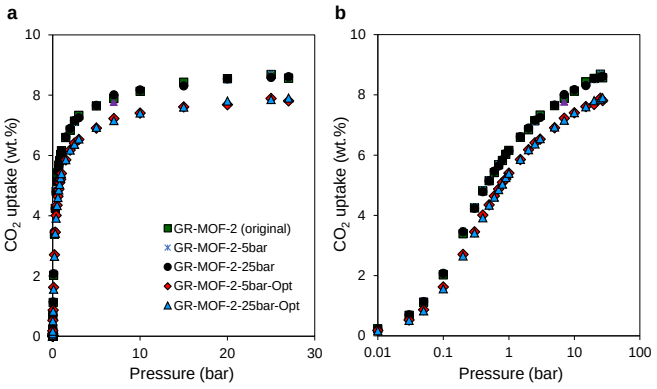

Fig. 5. Comparison of GCMC simulated CO_2 adsorption isotherms at 273 K on GR-MOF-2 and derived structures **a.** linear and **b.** semi-logarithmic scale

on the original **GR-MOF-2** and the four modified structures and the comparison of PSD. The modification of the unit cell parameters in structures GR-MOF-2-5bar and GR-MOF-2-25bar had no effect on the CO_2 uptake at any pressure, whereas the energy minimized structures presents a similar reduction of ca. 8%. All in all, this shows the lack of significant flexibility on this MOF, and therefore confirms the existence of a molecular sieve effect due to the presence of denser phases on the external surface of the powder material, where CO_2 – showing higher interaction with the MOF – is able to go through this layer and get adsorbed, but not CH_4 and/or H_2.

Conclusions

We report the synthesis of a new family of four new isoreticular metal-organic frameworks (MOFs) based on Cu-Cu paddle-wheel building units. The four MOFs contain 1D microchannels modulated by chemical functionalisation of the dicarboxylate ligand or the use of different bis-4,4'-pyridyl-like connectors behaving as ancillary linkers. Combining both experimental and grand canonical Monte Carlo isotherms as well as in-situ synchrotron X-ray diffraction, we show the adsorption behaviour towards CO_2, CH_4 and H_2, with some materials acting as molecular sieves with virtually infinite selectivity.

Experimental Section

Materials and physical measurements

All reagents were obtained from commercial sources and used as received. Elemental (C, H, and N) analyses were performed on a Leco CHNS-932 microanalyzer. IR spectra of powdered samples were recorded in the 400–4000 cm^{-1} region on a Nicolet 6700 FTIR spectrophotometer using KBr pellets.

Synthesis and fundamental characterization of GR-MOF compounds

All compounds were synthesized according to a general procedure by which a copper(II) salt, the corresponding dicarboxylic acid and 4,4'-bipy like linker were mixed in a 1:1:0.5 stoichiometric ratio and dissolved in a water/ethanol solution. Urea was added to deprotonate the dicarboxylic acid and to help in the formation of the complexes. The resulting mixtures gave rise to X-ray quality single crystals by slow evaporation.

*Synthesis of **GR-MOF-2**.*
The reaction solvent of the copper(II) sulfate (0.25 mmol, 0.0628 g), glutaric acid (0.25 mmol, 0.033 g), urea (0.872 mmol, 0.054 g) and azopyridine (0.125 mmol, 0.0231 g) in 20 mL of a water/ethanol (1:1) solvent mixture led to a blue solution. This solution was kept at room temperature for one week such that single crystals of **GR-MOF-2** were obtained, which were filtered off and air -dried. Yield: 60% (based on metal). Elemental analysis for $C_{10}H_{10}CuN_2O_6$ (321.77 g mol^{-1}). Calcd.: C, 37.80; H, 3.17; N, 8.82; Cu, 20.00. Experimental: C, 37.05; H, 3.31; N, 8.73; Cu, 19.90%.

*Synthesis of **GR-MOF-3**.*
0.25 mmol of copper(II) tetrafluoroborate (0.0628 g), 2-methylglutaric acid (0.25 mmol, 0.0365 g), urea (0.872 mmol, 0.054 g) and 1,4-bis(4-pyridyl)-2,3-diaza-1,3-butadiene (0.125 mmol, 0.0263 g) in 20 mL of a water/ethanol (1:1) solvent mixture led to a blue solution. This solution was kept at room temperature for one week such that single crystals of **GR-MOF-3** were obtained, which were filtered off and air -dried. Yield: 60% (based on metal). Elemental analysis for $C_{24}H_{36}Cu_2N_4O_{13}$ (715.64 g mol^{-1}). Calcd.: C, 40.28; H, 5.07; N, 7.83; Cu, 17.76. Experimental: C, 40.05; H, 5.22; N, 7.76; Cu, 18.01%.

*Synthesis of **GR-MOF-4**.*
0.25 mmol of copper(II) tetrafluoroborate (0.0628 g), 2,2'-dimethylglutaric acid (0.25 mmol, 0.0400 g), urea (0.872 mmol, 0.054 g) and 1,4-bis(4-pyridyl)-2,3-diaza-1,3-butadiene (0.125 mmol, 0.0263 g) in 20 mL of a water/ethanol (1:1) solvent mixture led to a blue solution. This solution was kept at room temperature for one week such that single crystals of **GR-MOF-4** were obtained, which were filtered off and air -dried. Yield: 60% (based on metal). Elemental analysis for $C_{13}H_{19}CuN_2O_6$ (362.84 g mol^{-1}). Calcd.: C, 43.03; H, 5.28; N, 7.72; Cu, 17.51. Experimental: C, 42.94; H, 5.33; N, 7.62; Cu, 17.65%.

*Synthesis of **GR-MOF-5**.*
The reaction solvent of the copper(II) nitrate (0.25 mmol, 0.0739 g), glutaric acid (0.25 mmol, 0.033 g), urea (0.872 mmol, 0.054 g) and 2,5-bis(4-pyridyl)-1,3,4-oxadiazole (0.125 mmol, 0.0280 g) in 20 mL of a water/ethanol (1:1) solvent mixture led to a blue solution. This solution was kept at room temperature for one week such that single crystals of **GR-MOF-5** were obtained, which were filtered off and air -dried. Yield: 60% (based on metal). Elemental analysis for $C_{22}H_{28}Cu_2N_4O_{13}$ (683.56 g mol^{-1}). Calcd.: C, 38.66; H, 4.13; N, 8.20; Cu, 18.59. Experimental: C, 38.55; H, 4.03; N, 8.15; Cu, 18.70%.

Crystallographic refinement and structure solution

Prismatic X-ray data collection of suitable single crystals of **GR-MOF-2**, **GR-MOF-3**, **GR-MOF-4** and **GR-MOF-5** were done at 100(2) K on a Bruker VENTURE area detector equipped with graphite monochromated Mo-Kα radiation (λ = 0.71073 Å) by applying the ω-scan method. The data reduction was performed with the APEX2[25] software and corrected for absorption using SADABS.[26] Crystal structures were solved by direct methods using the SIR97 program[27] and refined by full-matrix least-squares on F^2 including all reflections and using anisotropic displacement parameters by means of the WINGX crystallographic package (Table 2).[28] Hydrogen atoms belonging to ligands were geometrically refined with fixed contributions riding on attached atoms with isotropic thermal displacement parameters 1.2 times those of their parent atoms. Lattice solvent molecules could not be refined for **GR-MOF-3**, owing to their disordered disposition in the voids of the structures, so the electron density at the voids was subtracted from the reflection data by the SQUEEZE procedure as implemented in PLATON program[29] during the refinement. Moreover, during the refinement of **GR-MOF-3**, it was observed that error factors were unexpectedly high, which indicated the occurrence of twinning. Accordingly, it

was refined with the (0 1 2 / 0 –1 0 / 1 0 0) twin law and a final percentage of 10% for the minor domain. CCDC 1836112-1836115 contain the supplementary crystallographic data for this communication. These data can be obtained free of charge via http://www.ccdc.cam.ac.uk/conts/retrieving.html (or from the Cambridge Crystallographic Data Centre, 12, Union Road, Cambridge CB2 1EZ, UK; fax: +44 1223 336033). Crystallographic data are summarised in Table 2.

Table 2. Crystallographic data and structure refinement details of all compounds.

Compound	GR-MOF-2	GR-MOF-3	GR-MOF-4	GR-MOF-5
Chem. form.	$C_{10}H_{10}CuN_2O_6$	$C_{24}H_{36}Cu_2N_4O_{13}$	$C_{13}H_{19}CuN_2O_6$	$C_{22}H_{28}Cu_2N_4O_{13}$
Form. weight	321.77	715.64	362.84	683.56
Cryst. system	Monoclinic	Monoclinic	Monoclinic	Monoclinic
Space group	*C*2/c	*C*2/c	*C*2/c	*C*2/c
a (Å)	24.153(2)	27.019(9)	27.253(1)	26.9173(1)
b (Å)	13.120(1)	13.506(5)	13.608(1)	12.987(1)
c (Å)	8.600(1)	8.921(5)	9.146(2)	8.574(1)
β (º)	92.537(1)	94.792(6)	92.81(3)	104.82(1)
V (Å^3)	2722.4(5)	3244(2)	3387.8(7)	2897.5(3)
Z	8	4	8	4
GOF [a]	1.040	1.104	1.014	1.014
R_{int}	0.0361	0.0721	0.0929	0.0884
R_1 [b] / wR^2 [c] [I>2σ(I)]	0.0373 / 0.0882	0.0546 / 0.1548	0.0459 / 0.1046	0.0455 / 0.0973
R_1 [b] / wR^2 [c] (all data)	0.0492 / 0.0931	0.0707 / 0.1687	0.0734 / 0.1127	0.0812 / 0.1063

[a] $S = [\sum w(F_o^2 - F_c^2)^2 / (N_{obs} - N_{param})]^{1/2}$ [b] $R_1 = \sum||F_o|-|F_c|| / \sum|F_o|$ [c] $wR_2 = [\sum w(F_o^2 - F_c^2)^2 / \sum wF_o^2]^{1/2}$; $w = 1/[\sigma^2(F_o^2) + (aP)^2 + bP]$ where $P = (\max(F_o^2,0) + 2Fc^2)/3$ with a = 0.0469 (**GR-MOF-2**), 0.0936 (**GR-MOF-3**), 0.0612 (**GR-MOF-4**), 0.0509 (**GR-MOF-5**), and b = 22.4853 (**GR-MOF-3**), 2.6667 (**GR-MOF-5**).

In situ diffraction

Experiments were carried out at the Material Science beamline of the Swiss Light Source,[30] using a monochromated radiation of 0.77623 Å, as calibrated by the SRM640c Si standard from NIST. A gently ground powder sample of **GR-MOF-2** was inserted in a quartz glass capillary of 0.3 mm diameter, with wall thickness of 25 microns. The capillary was sealed into a locally constructed pressure system, heated by a cryojet under dynamic vacuum up to 120 C until no peak shift could be observed in diffraction. Diffracted signal was then collected at ambient temperature upon increasing CO_2 pressure using a Mythen-II 1D detector. The sample was gently rocked to ensure more uniform response, nevertheless the patterns are suffering from the granularity of the material, which could not be extensively ground to prevent loss of crystallinity. Therefore the patterns were Pawley fitted to obtain unit cell parameters using the program Topas.[31]

Gas Adsorption

The CH_4 (273 K), CO_2 (273 K) and H_2 (77 K) adsorption equilibrium isotherms were measured in a high-pressure volumetric adsorption system (up to 3 MPa) built for this purpose. The equipment consists of a stainless-steel volumetric adsorption apparatus equipped with mass flow and backpressure controllers to set the desired gas pressure in the system. Two MKS Baratron absolute pressure transducers are used to accurately measure the pressure in the range 0-1 bar and 1-32 bar. For each adsorption isotherm, approximately 0.2 g of the sample was degassed at 393 K for at least 12 h down to a pressure of 10^{-5} mbar. Then the sample container was set to the adsorption temperature and increasing doses of the adsorptive gas were admitted. Peng-Robinson equation applied to the adsorptive was used for the calculation of the adsorbed amount at each pressure, accounting for the non-ideality of the gases under the adsorption conditions. Isotherms are expressed as excess adsorbed amount as a function of the adsorptive pressure.

Computational Details.

Grand canonical Monte Carlo (GCMC) simulations were used to calculate the amount adsorbed for CO_2, CH_4 and H_2 at 273 K. The gas-gas and gas-framework interactions were modeled using Lennard-Jones (LJ) interactions. The LJ potential parameters for the framework atoms were taken from the Universal Force Field (UFF).[32] The interactions for CO_2,[33] CH_4[34] and H_2 were described by the TraPPE force field. An atomistic representation was used for the GR-MOFs, starting from its crystal structure. The simulation supercell consisted of 8 (2×2×3) unit cells with a LJ cut-off radius of 12.8 Å and no tail corrections. For CO_2 and H_2, the long-range electrostatic interactions were handled by the Ewald summation technique. Periodic boundary conditions were applied in all three dimensions. For each state point, GCMC simulations consisted of 20,000 Monte Carlo cycles to guarantee equilibration, followed by 20,000 production cycles to calculate the ensemble averages. All simulations included insertion/deletion, translation and rotation (for CO_2 and H_2) moves with equal probabilities.

All GCMC simulations were run on crystal structures obtained from PXRD. For **GR-MOF-2**, were ran simulations on different models: crystal structures obtained from PXRD at 5 bar and 25 bar and also structures where the atomic positions were subjected to geometry optimization based on molecular mechanics calculations. These calculations were performed with the Forcite module of Materials Studio,[35] using an algorithm that is a cascade of the steepest descent, adjusted basis set Newton–Raphson, and quasi-Newton methods. The bonded and the short-range (van der Waals) interactions between the atoms were modelled using the Universal Force Field (UFF). A cut-off distance of 18.5 Å was used for the van der Waals interactions during the geometry optimization.

Continuous shape measurements (CShMs)

Continuous shape measurements were performed by means of SHAPE program,[36] by which the shape of the polyhedron is compared to most common polyhedra containing five donor atoms.

Conflicts of interest

There are no conflicts to declare.

Acknowledgements

This work was supported by the Junta de Andalucía (FQM-1484), Red Guipuzcoana de Ciencia, Tecnolgía e Innovación (OF188/2017) and University of the Basque Country (GIU14/01, GIU17/013, EHUA16/32). The authors thank for technical and human support provided by SGIker of UPV/EHU and European funding (ERDF and ESF). D.F.-J. thanks the Royal Society for funding through a University Research Fellowship and the European Research Council (ERC) under the European Union's Horizon 2020 research and innovation programme (NanoMOFdeli), ERC-2016-COG 726380.

Notes and references

1 (a) E. D. Bloch, W. L. Queen, R. Krishna, J. M. Zadrozny, C. M. Brown and J. R. Long, *Science*, 2012, **335**, 1606. (b) A. Lan, K. Li, H. Wu, D. H. Olson, T. J. Emge, W. Ki, M. Hong and J. Li, *Angew. Chem., Int. Ed.*, 2009, **48**, 2334. (c) J.-Y. Lee, O. K. Farha, J. Roberts, K. A. Scheidt, S. Nguyen and J. T. Hupp, *Chem. Soc. Rev.*, 2009, **38**, 1450. (d) J. Cepeda, S. Pérez-Yáñez, G. Beobide, O. Castillo, E. Goikolea, F. Aguesse, L. Garrido, A. Luque and P. A. Wright, *Chem. Mater.*, 2016, **28**, 2519. (e) Y. Inokuma, S. Yoshioka, J. Ariyoshi, T. Arai, Y. Hitora, K. Takada, S. Matsunaga, K. Rissanen and M. Fujita, *Nature*, 2013, **495**, 461. (f) G. A. Craig and M. Murrie, *Chem. Soc. Rev.*, 2015, **44**, 2135. (g) T. Tian, Z. Zeng, D. Vulpe, M. E. Casco, G. Divitini, P. A. Midgley, J. Silvestre-Albero, J.-C. Tan, P. Z. Moghadam and D. Fairen-Jimenez, *Nature Materials*, 2018, **17**, 174. (h) M. H. Teplensky, M. Fantham, P. Li, T. C. Wang, J. P. Mehta, L. J. Young, P. Z. Moghadam, J. T. Hupp, O. K. Farha, C. F. Kaminski and D. Fairen-Jimenez, *J. Am. Chem. Soc*. 2017, **139**, 7522.

2 P. Z. Moghadam, A. Li, S. B. Wiggin, A. Tao, A. G. P. Maloney, P. A. Wood, S. C. Ward and D. Fairen-Jimenez, *Chem. Mater.*, 2017, **29**, 2618.

3 (a) O. K. Farha, I. Eryazici, N. C. Jeong, B. G. Hauser, C. E. Wilmer, A. A. Sarjeant, R. Q. Snurr, S. T. Nguyen, A. O. Yazaydin and J. T. Hupp, *J. Am. Chem. Soc.*, 2012, **134**, 15016. (b) J. R. Li, R. J. Kupler and H. C. Zhou, *Chem. Soc. Rev.*, 2009, **38**, 1477. (c) K. Sumida, D. L. Rogow, J. A. Mason, T. M. McDonald, E. D. Bloch, Z. R. Herm, T. H. Bae and J. R. Long, *Chem. Rev.*, 2012, **112**, 724.

4 (a) G. Férey, *Chem. Soc. Rev.*, 2008, **3**, 191. (b) M. Eddaoudi, D. F. Sava, J. F. Eubank, K. Adil and V. Guillerm, *Chem. Soc. Rev.*, 2015, **44**, 228. (c) H.-C. J. Zhou and S. Kitagawa, *Chem. Soc. Rev.*, 2014, **43**, 5415.

5 (a) M. O'Keeffe and O. M. Yaghi, *Chem. Rev.*, 2012, **112**, 675. (b) O. M. Yaghi, H. Li and T. L. Groy, *J. Am. Chem. Soc.*, 1996, **118**, 9096. (c) V. Guillerm, D. Kim, J. F. Eubank, R. Luebke, X. Liu, K. Adil, M. S. Lah and M. Eddaoudi, *Chem. Soc. Rev.*, 2014, **43**, 6141. (d) D. Fairen-Jimenez, Y.J. Colón, O.K. Farha , Y.-S. Bae, J.T. Hupp, R.Q. Snurr, *Chem. Commun*. 2012, **48**, 10496.

6 S. S. Y. Chui, S. M. F. Lo, J. P. H. Charmant, A. G. Orpen, I. D. Williams, *Science*, 1999, **283**, 1148.

7 (a) H. Chun, D. N. Dybtsev, H. Kim and K. Kim, *Chem. – Eur. J.*, 2005, **11**, 3521. (b) B. Fernández, J. M. Seco, J. Cepeda, A. J. Calahorro and A. Rodríguez-Diéguez, *CrystEngComm*, 2015, **17**, 7595. (c) H. J. Park and M. P. Suh, *Chem. Commun.*, 2010, **46**, 610.

8 (a) J. Goldsmith, A. G. Wong-Foy, M. J. Cafarella and D. J. Siegel, *Chem. Mater.*, 2013, **25**, 3373. (b) B. Chen, S. Ma, E. J. Hurtado, E. B. Lobkovsky and H. Zhou, *Inorg. Chem.*, 2007, **46**, 8490. (c) S. Pérez-Yáñez, G. Beobide, O. Castillo, M. Fischer, F. Hoffman, M. Fröba, J. Cepeda and A. Luque, *Eur. J. Inorg. Chem.*, 2012, 5921.

9 (a) S. Xiang, Y. He, Z. Zhang, H. Wu, W. Zhou, R. Krishna and B. Chen, *Nat. Commun.*, 2012, **3**, 954. (b) J. Cepeda, S. Pérez-Yáñez, G. Beobide, O. Castillo, M. Fischer, A. Luque and P. A. Wright, *Chem. – Eur. J.*, 2014, **20**, 1554.

10 (a) L. Kong, R. Zou, W. Bi, R. Zhong, W. Mu, J. Liu, R. P. S. Han and R. Zou, *J. Mater. Chem. A*, 2014, **2**, 17771. (b) Y.-S. Bae, B. G. Hauser, O. K. Farha, J. T. Hupp and R. Q. Snurr, *Microp. Mesop. Mater.*, 2011, **141**, 231. (c) B. Chen, S. Ma, F. Zapata, F. R. Fronczek, E. B. Lobkovsky and H. Zhou, *Inorg. Chem.*, 2007, **46**, 1233.

11 (a) M. Paik Suh, H. J. Park, T. K. Prasad and D.-W. Lim, *Chem. Rev.*, 2012, **112**, 782. (b) S.-Y. Zhang, X. Zhang, H. Li, Z. Niu, W. Shi and P. Cheng, *Inorg. Chem.*, 2015, **54**, 2310.

12 D. Fairen-Jimenez, N. A. Seaton and T. Düren, *Langmuir*, 2010, **26**, 14694.

13 (a) A. R. Millward and O. M. Yaghi, *J. Am. Chem. Soc.*, 2005, **127**, 17998. (b) J. Getzschmann, I. Senkovska, D. Wallacher, M. Tovar, D. Fairen-Jimenez, T. Düren, J. M. van Baten, R. Krishna and S. Kaskel, *Microp. Mesop. Mater.*, 2010, **136**, 50.

14 (a) B. Fernández, G. Beobide, I. Sánchez, F. Carrasco-Marín, J. M. Seco, A. J. Calahorro, J. Cepeda and A. Rodríguez-Diéguez, *CrystEngComm*, 2016, **18**, 1282. (b) N. Nijem, H. Wu, P. Canepa, A. Marti, K J. Balkus, T. Thonhauser, J. Li and Y. J. Chabal, *J. Am. Chem. Soc.*, 2012, **134**, 15201.

15 (a) E. J. Carrington, C. A. McAnally, A. J. Fletcher, S. P. Thompson, M. Warren and L. Brammer, *Nat. Chem.*, 2017, **9**, 882. (b) K. Uemura, R. Matsuda and S. Kitagawa, *J. Solid State Chem.*, 2005, **178**, 2420. (c) N. A. Ramsahye, G. Maurin, S. Bourrelly, P. L. Llewellyn, T. Loiseau, C. Serre and G. Férey, *Chem. Commun.*, 2007, 3261. (d) P. Z. Moghadam, J. F. Ivy, R. K. Arvapally, A. M. dos Santos, J. C. Pearson, L. Zhang, E. Tylianakis, P. Ghosh, I. W. H. Oswald, U. Kaipa, X. Wang, A. K. Wilson, R. Q. Snurr and M. A. Omary, *Chem. Sci*., 2017, **8**, 3989.

16 (a) D. Fairen-Jimenez, S. A. Moggach, M. T. Wharmby, P. A. Wright, S. Parsons and T. Düren, *J. Am. Chem. Soc*., 2011, **133**, 8900. (b) D. Fairen-Jimenez, R. Galvelis, A. Torrisi, A. D. Gellan, M. T. Wharmby, P. A. Wright, C. Mellot-Draznieks and T. Düren, *Dalton Trans.*, 2012, **41**, 10752.

17 J. M. Seco, D. Fairén-Jimenez, A. J. Calahorro, L. Méndez-Liñán, M. Pérez-Mendoza, N. Casati, E. Colacio and A. Rodríguez-Diéguez, *Chem. Commun.*, 2013, **49**, 11329.

18 (a) C. Herdes and L. Sarkisov, *Langmuir*, 2009, **25**, 5352. (b) L. Sarkisov and A. Harrison, *Mol. Simul.*, 2011, **37**, 1248.

19 (a) J. Cepeda, S. Pérez-Yáñez, G. Beobide, O. Castillo, M. Fischer, A. Luque and P. A. Wright, *Chem.–Eur. J.*, 2014, **20**, 1554. (b) J. Thomas-Gipson, R. Pérez-Aguirre, G. Beobide, O. Castillo, A. Luque, S. Pérez-Yáñez and P. Román, *Cryst. Growth Des.*, 2015, **15**, 975.

20 (a) R. Dey, R. Haldar, T. K. Maji and D. Ghoshal, *Cryst. Growth Des.*, 2011, **11**, 3905. (b) C. X. Bezuidenhout, V. J. Smith, P. M. Bhatt, C. Esterhuysen and L. J. Barbour, *Angew. Chem., Int. Ed.*, 2015, **54**, 2079.

21 J. I. Feldblyum, M. Liu, D. W. Gidley and A. J. Matzger, *J. Am. Chem. Soc.*, 2011, **133**, 18257.

22 (a) T. Loiseau, L. Lecroq, C. Volkringer, J. Marrot, G. Férey, M. Haouas, F. Taulelle, S. Bourrelly, P. L. Llewellyn and M. Latroche, *J. Am. Chem. Soc.*, 2006, **128**, 10223. (b) S. Surblé, F. Millange, C. Serre, T. Duren, M. Latroche, S. Bourrelly, P. L. Llewellyn and G. Férey, *J. Am. Chem. Soc.*, 2006, **128**, 14889.

23 (a) R. Matsuda, R. Kitaura, S. Kitagawa, Y. Kubota, T. C. Kobayashi, S. Horike and M. Takata, *J. Am. Chem. Soc.*, 2004, **126**, 14063. (b) Y.-S. Bae, A. Yazaydin and R. Q. Snurr, *Langmuir*, 2010, **26**, 5475. (c) D. Bradshaw, J. E. Warren and M. J. Rosseinsky, *Science*, 2007, **315**, 977. (d) R. Kitaura, K.

Seki, G. Akiyama and S. Kitagawa, *Angew. Chem., Int. Ed.*, 2013, **42**, 428.
24 G. Barin, V. Krungleviciute, O. Gutov, J. T. Hupp, T. Yildirim and O. K. Yaghi, *Inorg. Chem.*, 2014, **53**, 6914.
25 Bruker Apex2, Bruker AXS Inc., Madison, Wisconsin, USA, 2004.
26 G.M. Sheldrick, SADABS, Program for Empirical Adsorption Correction, Institute for Inorganic Chemistry, University of Gottingen, Germany, 1996.
27 A. Altomare, M. C. Burla, M. Camilla, G. L. Cascarano, C. Giacovazzo, A. Guagliardi, A. G. G. Moliterni, G. Polidori and R. Spagna, *J. Appl. Cryst*., 1999, **32**, 115.
28 (a) G. M. Sheldrick, SHELX-2014, Program for Crystal Structure Refinement, University of Göttingen, Göttingen, Germany, 2014. (b) L. J. Farrugia, *J. Appl. Cryst*., 1999, **32**, 837.
29 A. L. Spek, *J. Appl. Crystallogr.*, 2003, **36**, 7.
30 P. R. Willmott, D. Meister, S. J. Leake, M. Lange, A. Bergamaschi, M. Boege, M. Calvi, C. Cancellieri, N. Casati, A. Cervellino, Q. Chen, C. David, U. Flechsig, F. Gozzo, B. Henrich, S. Jaeggi-Spielmann, B. Jakob, I. Kalichava, P. Karvinen, J. Krempasky, A. Ludeke, R. Luscher, S. Maag, C. Quitmann, M. L. Reinle-Schmitt, T. Schmidt, B. Schmitt, A. Streun, I. Vartiainen, M. Vitins, X. Wang and R. Wullschleger, *J. Synchrotron Rad*., 2013, **20**, 667.
31 Topas 5, Bruker AXS.
32 A. K. Rappe, C. J. Casewit, K. S. Colwell, W. A. Goddard and W. M. Skiff, *J. Am. Chem. Soc*., 1992, **114**, 10024.
33 J. J. Potoff, J. I. Siepmann, *Alche Journal*, 2001, **47**, 1676.
34 M. G. Martin. J. I. Siepmann, *J. Phys. Chem. B*, 1998, **102**, 2569.
35 Materials Studio 5.0; Accelrys Software Inc.: San Diego, CA, 2009.
36 M. Llunell, D. Casanova, J. Cirera, J. M. Bofill, P. Alemany, S. Alvarez, M Pinsky and D. Avnir, SHAPE v1.7, University of Barcelona, Barcelona, 2010.